AIAA SciTech Forum
January 3-7, 2022, San Diego, CA & Virtual
AIAA SCITECH 2022 Forum

10.2514/6.2022-0640

Effect of O_2/CO_2 ratio on stability and near field structure of oxyfuel jet diffusion flames at atmospheric pressure.

Muhammad Bukar[1], Suman Basnet[1], Taesung Kim[2], Gaetano Magnotti[3]

Physical Science and Engineering Division, Clean Combustion Research Center, King Abdullah University of Science and Technology, Thuwal 23955, Saudi Arabia

This paper presents an experimental study on the stability and structure of non-premixed CO_2 diluted oxyfuel jet flames. DSLR imaging and OH Planar Laser-Induced Fluorescence (PLIF) were used to investigate the nearfield structure of a series of methane jet flames. Three oxidizer compositions (O_2/CO_2 ratios of 50/50, 40/60, and 32/68) were considered for a fixed co-flow velocity of 0.35 m/s. The PLIF Images were post-processed using MATLAB to obtain OH layer thickness, flame attachment height, and radius. Results show that increasing the CO_2 level in the co-flow leads to a reduction in the OH layer thickness and sooting propensity. Both attachment radius and height were found to increase with increased CO_2 content in the oxidizer. Furthermore, it was also observed that the flame attachment radius decreased as jet velocity increased while the flame attachment height tended to increase with higher jet velocity.

Nomenclature

U_{jet}	=	Fuel jet velocity (m/s)
$U_{co\text{-}flow}$	=	Coflow velocity (m/s)
U_{lift}	=	Lift off velocity
f	=	Focal length (mm)
Zst	=	Stoichiometric mixture fraction
δ	=	Burner lip thickness
d_i	=	Fuel tube inner diameter
h_a	=	Flame attachment height (mm)
r_a	=	Flame attachment radius (mm)
α	=	Jet spreading angle

I. Introduction

As the global demand for energy rises, there is a corresponding increase in awareness about the impact of human-induced emissions, especially of CO_2, on our planet. Currently, the concentration of CO_2 in the atmosphere is above 400 parts per million (ppm). This concentration is higher than at any point in the past 400,000 years [1]. It is generally accepted that the dramatic increase is due to anthropogenic activities. Some have estimated that by 2050 if current behaviors persist, the level of atmospheric CO_2 will increase by about 70% compared to current levels[2].

Fossil fuel combustion in the power production sector contributes about 40% of the emissions[3], prompting governments and industries to turn their attention to alternative energy sources such as renewables. However, fossil

[1] Graduate Student.
[2] Postdoctoral fellow.
[3] Assistant Professor.

fuel combustion will still play a significant role in the foreseeable future due to its ubiquity. However, the use of fossil fuels must be accompanied by new technologies that can help mitigate emissions into the atmosphere.

Oxyfuel combustion, using CO_2 as the diluent, can greatly simplify emission reduction and carbon capture strategies in fossil fuel combustion applications, as in principle NO_X cannot be formed, and CO_2 and water are the only combustion products. In particular, novel power cycles such as the Allam cycle [4] use supercritical CO_2 (sCO_2) as working fluid and high-pressure oxyfuel combustion to eliminate emissions in power production while maintaining a 59% thermodynamic efficiency, comparable to state-of-the-art combined cycles gas turbines [5]. The combustor employed in the Allam cycle operates at a pressure of about 300 bar, which is radically different from the pressures encountered in typical gas turbines. But as of now, turbulent flames at very high pressures (more than 100 bar) have barely been explored due to the difficulty of reproducing such conditions at a laboratory scale. Several numerical studies[6-8] have been conducted (both LES and RANS) reproducing conditions encountered in the Allam cycle, but they employ kinetics and mixing models that have not been validated by experimental results[9]. Therefore experimental data at conditions relevant to the Allam cycle are greatly needed to improve the quality of simulations and help industries improve their combustor design capability.

Several studies have been undertaken on oxy-combustion in CO_2 in recent years but at atmospheric pressures. For example, Yang et al. [10] applied 2D OH* imaging to study the effect of changing O_2/CO_2 ratio on the reaction zone and structural characteristics of pure methane flames in a CO_2 diluted co-flow and compared the results to an environment with nitrogen as diluent. They found that the CO_2 flames had a narrower flame front for the same diluent concentration than N_2 flames. Other studies focused on the effect of CO_2 on chemical kinetics[11], flame stability[12], adiabatic flame temperature[13], and laminar burning velocity[14].

This work focuses on the stability and the nearfield flame structure of a chambered diffusion jet oxyfuel flame in an O_2/CO_2 coflow, operated at atmospheric pressure. The details of the burner can be found in section II. The burner geometry was designed to operate at a high-pressure environment once installed in a suitable high-pressure vessel (which is currently under development). Results at atmospheric pressure for varying oxidizer composition (O_2/CO_2 ratio) and fuel velocity provide a baseline for the operation of the burner and guidelines for the design of the vessel for high-pressure operation.

II. Experimental Setup

A. Burner description

Figure 1 shows a schematic illustration of the co-flow burner employed for this study. The burner consists of a central jet of gaseous fuel, co-flow of O_2/CO_2, and a dilution stream consisting of N_2. The inner and outer diameters of the fuel tube are 1.75 mm and 3.18 mm, respectively. The burner lip thickness, δ, is 0.7 mm. The fuel tube and the oxidizer co-flow are enclosed in a quartz confinement with a square cross-section (25 mm x 25 mm), 150 mm tall. A larger optical (40 mm x 40 mm cross-section and 200 mm tall) enclosure surrounds the dilution stream. We opted for a square cross-section for enclosures to get lower-cost, high-quality quartz, avoid image distortions and ultimately achieve higher spatial resolutions. The enclosure side walls are 2 mm thick UV fused silica windows. An electric heater is also available to increase the temperature of the co-flow and of the outer dilution flow, but it was not employed in this experiment. The heated dilution co-flow can minimize heat losses through the burner and provide more controlled boundary conditions.

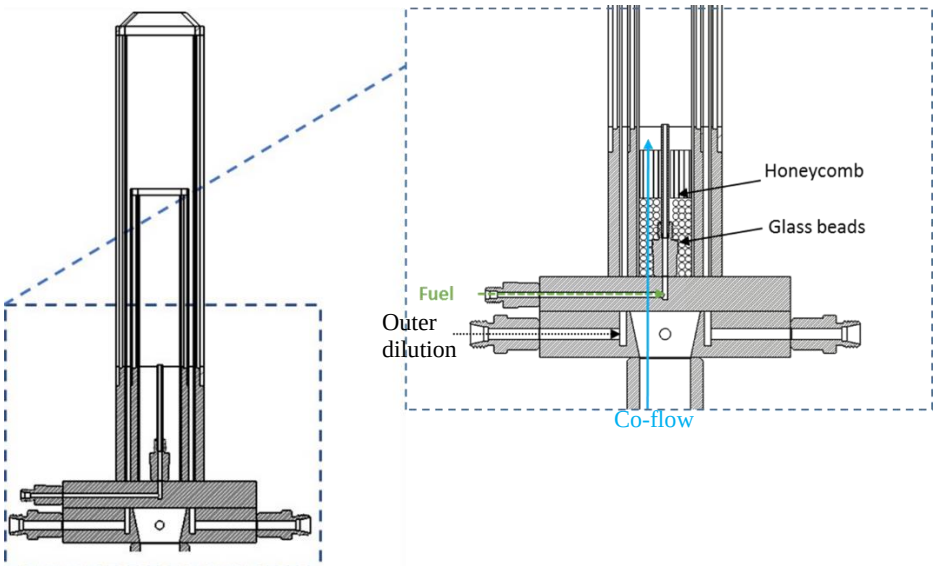

Figure 1: Co-flow burner configuration

The gas flow rates were controlled using MKS and Brooks mass flow controllers (MFC) operated between 10% and 90% of their full-scale capacity. Flowmeters were calibrated using a Drycal flow calibrator with a nominal accuracy of 0.5%.

B. Diagnostic

OH Planar Laser Induced-Fluorescence (PLIF) was used to characterize the flame structure throughout this study. The schematic of the PLIF system is shown in Figure 2. An Nd: YAG laser (Continuum, Powerlite DLS9010) pumps a dye laser (Continuum, ND6000 + UVT) at a repetition rate of 10 Hz. The dye laser was tuned to get a wavelength of 283.927 nm in order to excite the $Q_1(6) line\ of\ the\ OH\ X^2\Pi - A^2\Sigma^+\ (1,0)$ transition. The laser output energy was about 7 mJ/pulse. The laser was then re-directed through sheet-forming optics (LaVision sheet optics (VZ11) which focused the laser beam to a sheet 50 mm tall.

The PLIF signal collection system consisted of a bandpass filter centered at 309 nm (±5 nm), a 100 mm UV lens (with f/2.8), and a16-bit intensified PI-MAX3 CCD (1024x1024) camera operated with a gating time of 250 ns. The PLIF images have a pixel resolution of 0.029 mm/pixel

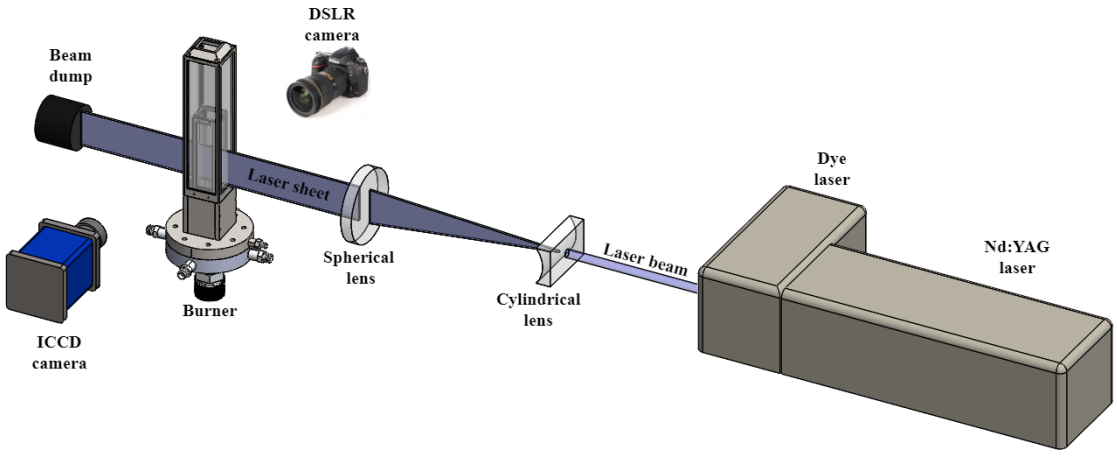

Figure 2: Burner with OH-PLIF optical setup

C. Flame conditions

Table 1 summarizes the test cases used for this study. The parameters of interest are the co-flow composition (different O_2/CO_2 ratios and air) and the fuel jet exit velocity. For each co-flow composition, the co-flow velocity was set to 0.35 m/s. The fuel jet velocity was varied from 10 m/s to about 90% of the lift-off condition, with steps of 10 m/s.

Co-flow composition [%]	O_2/CO_2 = 50/50	O_2/CO_2 = 40/60	O_2/CO_2 = 32/68	air
Jet fuel velocity [m/s]	10, 20, 30, 40, 50, 60	10, 20, 30, 40	10, 20	10, 20

Table 1: Test matrix with co-flow composition and fuel exit mean velocity. The fuel is methane, and in all cases, co-flow velocity was fixed to 0.35 m/s.

D. Image Processing

The OH-PLIF images obtained with ICCD camera were post-processed with MATLAB. For each flame test case, a set of 100 images were acquired for the analysis. First of all, the raw images were background-subtracted and then normalized by the maximum signal intensity. After that, the edge of the OH layer was detected using the Canny Edge algorithm[15], which determines the edge based on the local maxima of the gradient. Figure 3 shows the edge detected for three different jet velocities (U_{jet} = 10, 30 and 60 m/s) for fixed co-flow composition (O_2/CO_2 = 50/50) and velocity ($U_{co\text{-}flow}$ = 0.35 m/s). The instantaneous attachment height and radius were computed as the distance of the lower tip of the OH-edge from the burner surface and the burner centerline, respectively (see Fig. 4). The flames present small asymmetries, and the attachment height and radius reported here are computed for the side of the flame closer to the laser.

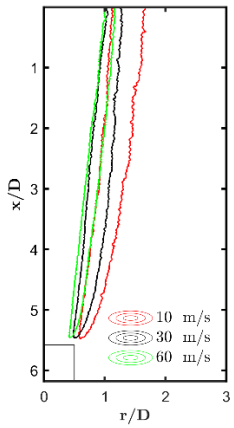

Figure 3: OH edge detected by Canny algorithm for $U_{co\text{-}flow}$ = 0.35 m/s and O_2/CO_2 concentration in the coflow of 50/50.

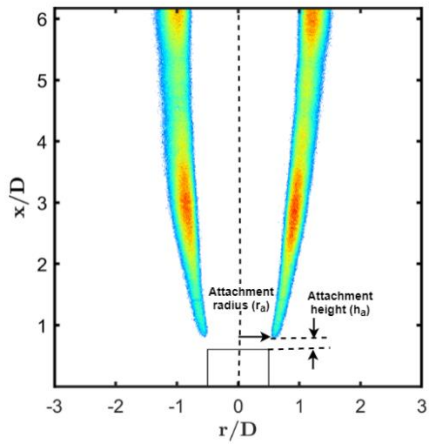

Figure 4: Illustration of attachment height and attachment radius detection from OH-PLIF images.

III. Results and Discussions

A. Effect of O_2/CO_2 ratio on flame stability.

Flame stability studies are useful because they essentially define the operational limits of a combustion system. Several papers [16-18] have been published on the stabilization mechanism of diffusion flames in a jet flame configuration. These stability limits are usually defined in terms of "lift-off," "reattachment," and "blowoff" velocities. A flame is said to be lifted when it stabilizes at a location downstream of the fuel nozzle tip when its jet becomes higher than a critical value (i.e., the lift-off velocity). Blowoff occurs when a flame extinguishes from an attached state.

In this campaign, our co-flow burner's lift-off stability is investigated for three oxidizer compositions (O_2/CO_2 ratio of 50/50, 40/60, and 32/68), as well as air. 32/68 of O_2/CO_2 mixture concentration matches the adiabatic flame temperature obtained for air as co-flow. The oxidizer co-flow velocity is increased up to 1.0 m/s at various intervals for the various oxidizer compositions considered. Figure 5 shows the plot of the lift of velocity as a function of the coflow velocity. Figure 5 shows that the lift-off velocity increases with the O_2 content. We can also observe from the plot a striking similarity between the U_{lift} curves for air and the 32/68 cases. The 32/68 O_2/CO_2 case and the air coflow case share the same adiabatic temperature but very different laminar flame speeds (21.3 cm/s and 38.2 cm/s, respectively. The lift-off velocity strongly decreases with the co-flow velocity for the air and 32/68 O_2/CO_2 cases, but small changes are observed for the 40/60 and 50/50 cases. The co-flow dependence is caused by the contribution of the entrained co-flow to the velocity at the stabilization point. This effect can be accounted for by plotting the results in terms of an effective velocity defined as: $\boldsymbol{U_{eff} = U_{jet} + \left(\frac{1-Z_{stoich}}{Z_{stoich}}\right)}$ where $\boldsymbol{Z_{stoich}}$ is the stoichiometric mixture fraction[19].

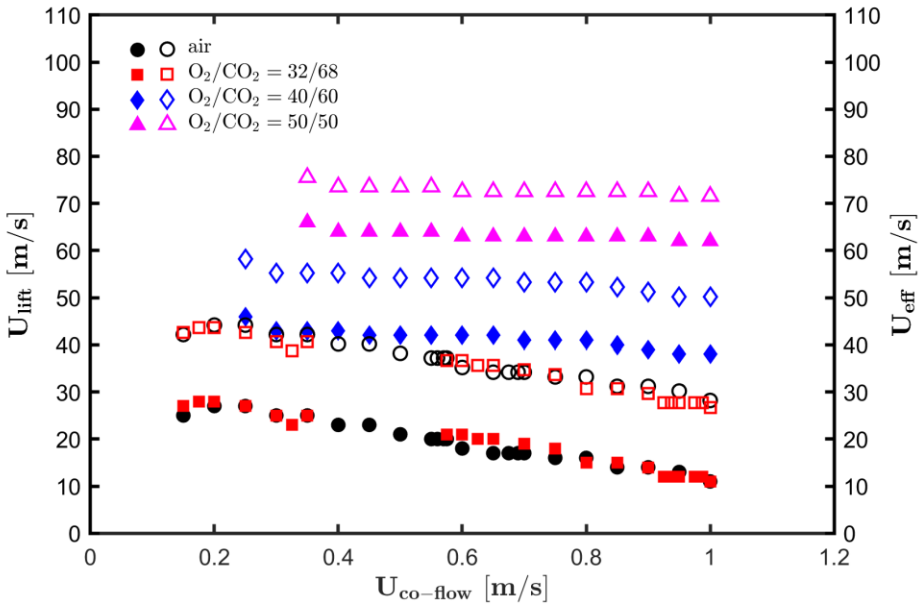

Figure 5: Plot of U_{lift} and against coflow velocity for four oxidizer compositions. The thick points represent the U_{lift} value while the hollow data points are for the U_{eff}.

B. DSLR and PLIF images of attached flames

DSLR and instantaneous PLIF images of some of the conditions described in Table 1 are shown in Fig. 6. The co-flow velocities were kept constant, while the percentage of CO_2 in the co-flow was increased from 50% to 68%. The baseline air case is also shown for comparison. The DSLR images show that the soot formation is suppressed with an increase of CO_2 dilution. This result is consistent with several studies that show that more CO_2 tends to break soot propensity in hydrocarbon flames [20-22]. The behavior is attributed to both chemical[22] and thermal effects of CO_2 dilution. We also notice that at a fixed coflow composition, a reddish zone is observed at the low fuel velocity at the center of the flame. The center red flame disappears with an increase in the fuel velocity because the mixing between the fuel and co-flow is enhanced. The OH PLIF images show that the thickness of the OH layer becomes thinner with increased levels of CO_2. At a fixed coflow composition, an increase in the jet velocity also causes the OH PLIF to become thinner. This effect is explained further in section III (C).

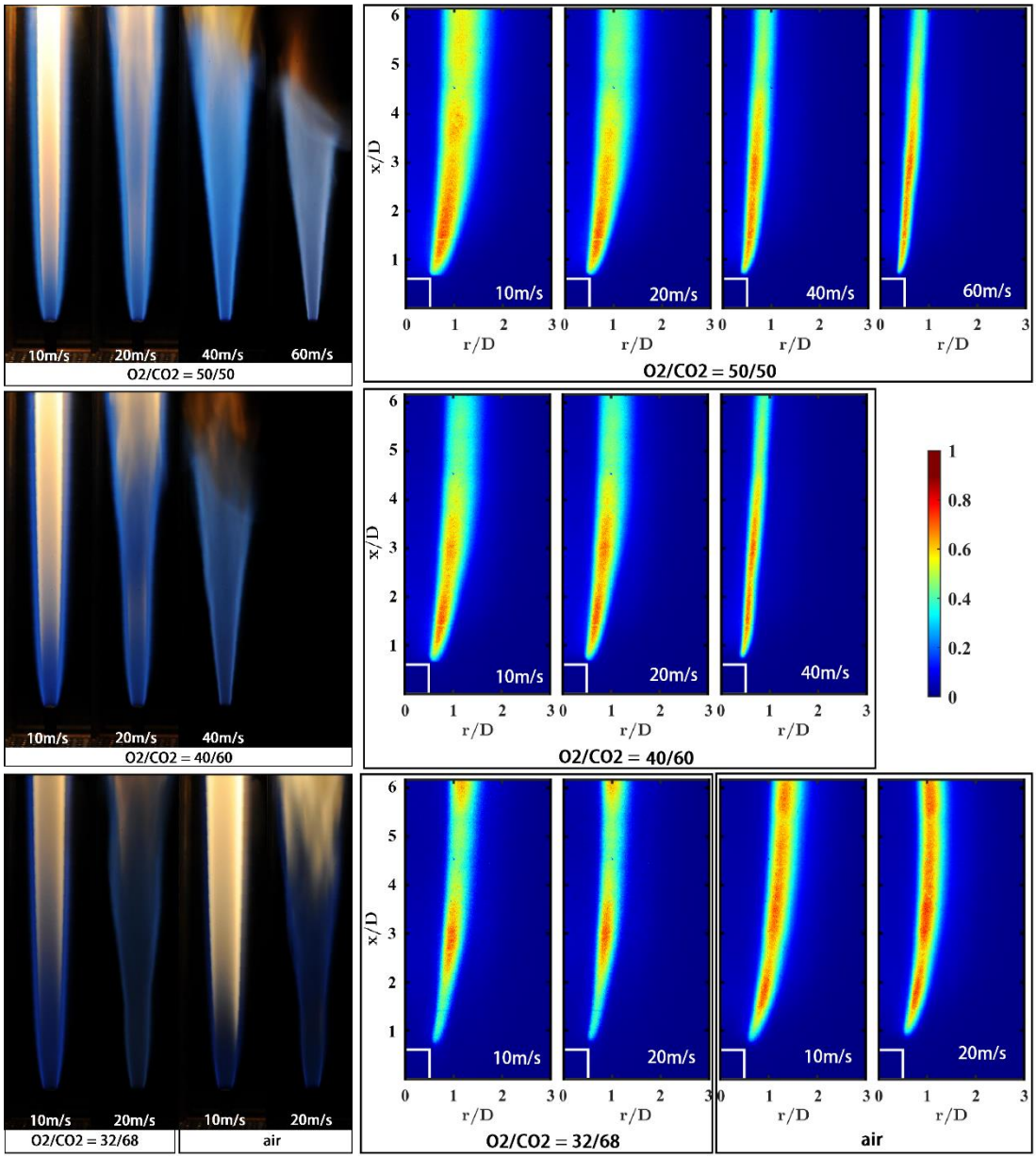

Figure 6: DSLR (left) and OHPLIF (right) images of the attached flames with $U_{co\text{-}flow}$ = 0.35 m/s. The co-flow composition and the fuel jet velocity are varied. Note that the OHPLIF images are of near field, and the rectangle indicates the location of the fuel tube. The numbers underneath the images represent U_{jet}

B. Flame Attachment Location

A flame stabilizes in the near-stoichiometric premixed region near the flame base location, where the laminar flame speed is balanced by the flow speed [17, 23]. Figure 7 shows the flame attachment location in terms of attachment height (h_a) and radius (r_a). For increasing fuel velocity, the attachment height increases for all oxidizers composition tested. As the fuel jet exit velocity increases, the distance needed to decelerate to the laminar flame speed increases, explaining the increase in the attachment height. The effect is enhanced by reducing the O_2/CO_2 ratio, as shown by the increase in the slope of the attachment height plotted as a function of the fuel velocity.

Additionally, for an assigned fuel jet velocity, figure 7 (a) shows that increasing the percentage of CO_2 in the oxidizer moves the flame's stabilization point away from the nozzle (i.e., higher h_a). This happens because the laminar flame speed decreases with increased CO_2 concentration, as shown by several numerical and experimental studies [14, 24-26].

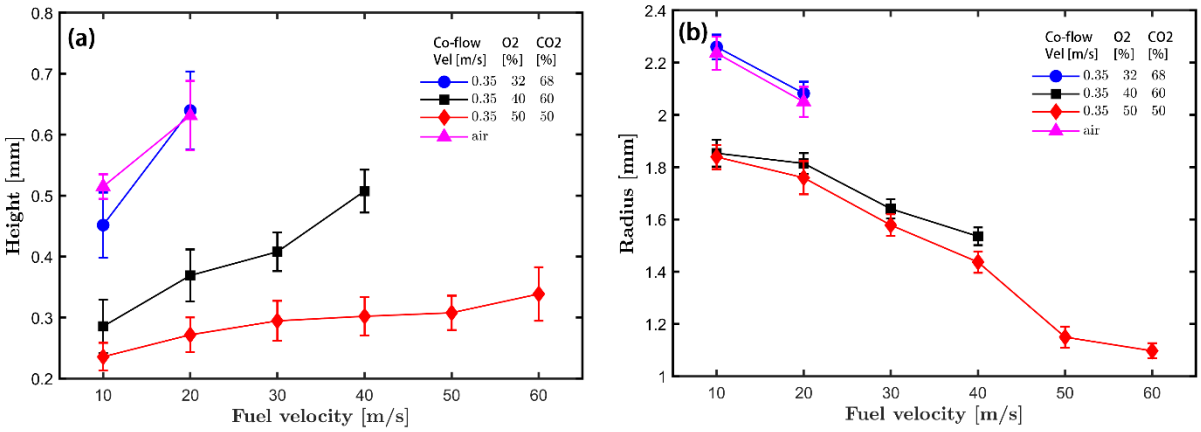

Figure 7: Attachments height and radius as function U_{jet}. Error bars shown represent the standard deviation

Figure 7 (b) shows that jet velocity increase leads to a reduction in the attachment radius for all co-flow compositions. This behavior is attributed to increased entrainment of the co-flow oxidizer at higher jet velocities, leading to smaller spreading angles, moving the stoichiometric line toward the nozzle centerline. This trend has been observed in a couple of other studies as well[23, 27]. Figure 7 (b) also shows that increasing CO_2 concentration while leaving other parameters constant increases the attachment radius. The decrease in attachment radius with increased O_2/CO_2 can be ascribed to the change in the stoichiometric mixture fraction Zst. Increasing the O_2 content requires more fuel to reach stoichiometry, therefore pulling the stoichiometric contour toward the centerline. Figure 8 shows the attachment radius normalized by the burner thickness plotted against Zst for a jet velocity of 20 m/s.

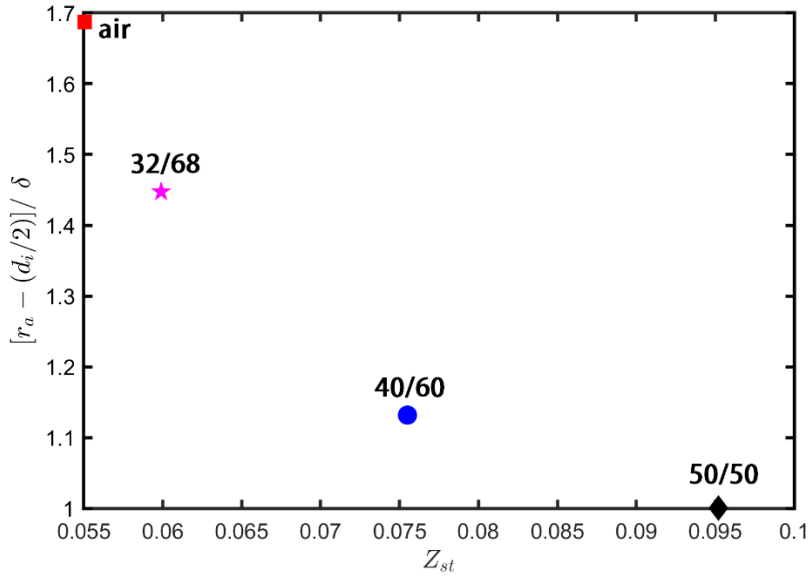

Figure 8: Plot of r_a normalized by the burner lip thickness against Z_{st}

C. OH Layer thickness

Figure 9 shows the OH layer thickness calculated for the various conditions considered. We can see that the OH layer decreases almost linearly with increasing jet velocity for all co-flow compositions. This trend is perhaps due to the higher strain rates encountered as we increase the jet velocity, decreasing OH thickness[28, 29]. We also notice that increasing the CO_2 percentage in the co-flow decreases the OH layer thickness. For U_{jet}= 10 m/s and $U_{co\text{-}flow}$ = 0.35 m/s, we see that increasing the CO_2 percentage from 50 to 68 reduces the OH layer thickness by almost half. This effect is likely due to decreased adiabatic flame temperature associated with increased CO_2 mole fraction in the oxidizer. In an opposed diffusion flame configuration, 1D laminar flame calculations using Chemkin PRO and GRI 3.0 mechanism show that increasing CO_2 in the oxidizer leads to a decrease in OH thickness (see Fig. 10). It could also be due to the effect of strain rate, as explained previously.

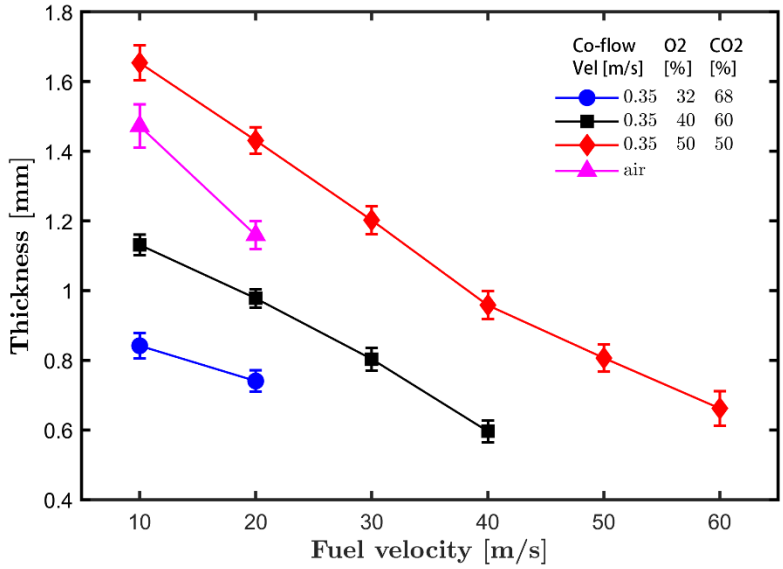

Figure 9: Plot OH layer thickness as a function of U_{fuel} and co-flow composition. Error bars shown represent the standard deviation of the 100 images taken.

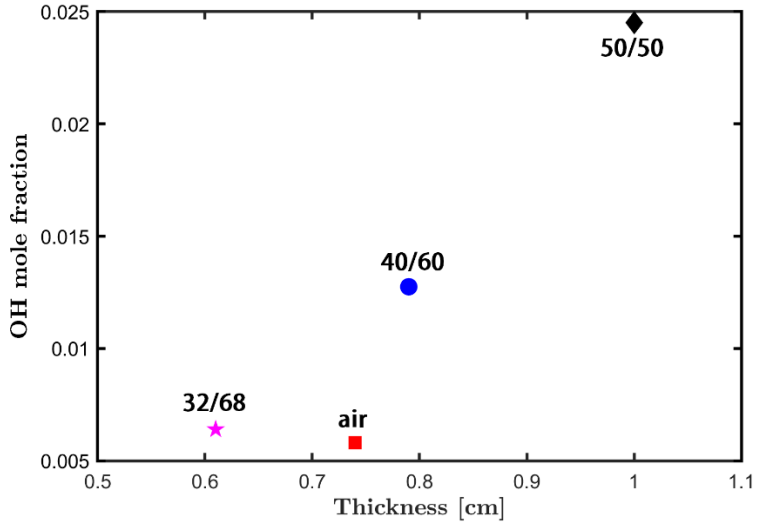

Figure 10: Plot of OH layer thickness from 1D counterflow chemkin simulations for various O_2/CO_2 ratios

IV. Conclusion

This work investigates the nearfield structure of oxyfuel jet diffusion flames using OH PLIF and DSLR imaging. The instantaneous flame attachment location and OH layer thickness were calculated for pure methane flames with different levels of CO_2 dilution in the coflow. Results show that attachment radius and the OH layer thickness decreased with fuel jet velocity for all coflow compositions considered. However, increasing the percentage of CO_2 in the coflow increases the attachment radius while decreasing the OH layer thickness. On the other hand, the attachment height increases with increased fuel jet velocity at fixed co-flow compositions. However, an increase in the CO_2 content in the oxidizer causes the attachment height to decreases

Acknowledgments

The work presented in this paper is funded by King Abdullah University of Science and Technology (KAUST)

References

[1] X. Huang, J. Guo, Z. Liu, C. Zheng, Opportunities and challenges of oxyfuel combustion, in: Oxy-Fuel Combustion, Elsevier, 2018, pp. 1-12.
[2] M. Lupion, R. Diego, L. Loubeau, B. Navarrete, Energy Procedia, 4 (2011) 5639-5646.
[3] Z. Li, A. Cuoci, A. Sadiki, A. Parente, Energy, 139 (2017) 555-570.
[4] R. Allam, J. Fetvedt, B. Forrest, D. Freed, in: ASME turbo expo 2014: turbine technical conference and exposition, American Society of Mechanical Engineers Digital Collection, 2014.
[5] R. Allam, S. Martin, B. Forrest, J. Fetvedt, X. Lu, D. Freed, G.W. Brown Jr, T. Sasaki, M. Itoh, J. Manning, Energy Procedia, 114 (2017) 5948-5966.
[6] D.T. Banuti, L. Shunn, S. Bose, D. Kim, in: The 6th International Symposium on Supercritical CO2 Power Cycles, 2018.
[7] J. Delimont, N. Andrews, L. Chordia, in: Turbo Expo: Power for Land, Sea, and Air, American Society of Mechanical Engineers, 2018, pp. V009T038A025.
[8] G. Indelicato, P.E. Lapenna, R. Concetti, M. Caputo, M. Valorani, G. Magnotti, F. Creta, Combustion Science and Technology, 192 (11) (2020) 2028-2049.
[9] P.A. Strakey, Journal of Energy Resources Technology, 141 (7) (2019).
[10] J. Yang, Y. Gong, Q. Guo, H. Zhu, L. He, G. Yu, Exp. Therm Fluid Sci., 108 (2019) 16-24.
[11] P. Glarborg, L.L. Bentzen, Energy Fuels, 22 (1) (2008) 291-296.
[12] P. Kutne, B.K. Kapadia, W. Meier, M. Aigner, Proc. Combust. Inst., 33 (2) (2011) 3383-3390.
[13] C. Liu, G. Chen, N. Sipöcz, M. Assadi, X.-S. Bai, Applied Energy, 89 (1) (2012) 387-394.
[14] A.N. Mazas, D.A. Lacoste, T. Schuller, in: ASME Turbo Expo 2010: Power for Land, Sea, and Air, 2010, pp. 411-421.
[15] L. Ding, A. Goshtasby, Pattern Recognit., 34 (3) (2001) 721-725.
[16] S. Lamige, J. Min, C. Galizzi, F. André, F. Baillot, D. Escudié, K.M. Lyons, Combust. Flame, 160 (6) (2013) 1102-1111.
[17] F. Takahashi, M. Mizomoto, S. Ikai, N. Futaki, in: Symposium (International) on Combustion, Elsevier, 1985, pp. 295-302.
[18] F. Takahashi, W.J. Schmoll, V.R. Katta, in: Symposium (International) on Combustion, Elsevier, 1998, pp. 675-684.
[19] T.F. Guiberti, W.R. Boyette, A.R. Masri, W.L. Roberts, Combust. Flame, 203 (2019) 301-312.
[20] H.I. Joo, Ö.L. Gülder, Combust. Flame, 157 (6) (2010) 1194-1201.
[21] A.E. Karataş, Ö.L. Gülder, Fuel, 200 (2017) 76-80.
[22] F. Liu, H. Guo, G.J. Smallwood, Ö.L. Gülder, Combust. Flame, 125 (1-2) (2001) 778-787.
[23] M. Marin, F. Baillot, Combust. Flame, 171 (2016) 264-280.

[24] B. Galmiche, F. Halter, F. Foucher, P. Dagaut, Energy Fuels, 25 (3) (2011) 948-954.
[25] E. Hu, X. Jiang, Z. Huang, N. Iida, Energy Fuels, 26 (7) (2012) 4242-4252.
[26] L. Qiao, Y. Gan, T. Nishiie, W.J. Dahm, E.S. Oran, Combust. Flame, 157 (8) (2010) 1446-1455.
[27] Y. Otakeyama, T. Yokomori, M. Mizomoto, Proc. Combust. Inst., 32 (1) (2009) 1091-1097.
[28] J.S. Park, D.J. Hwang, J. Park, J.S. Kim, S. Kim, S.I. Keel, T.K. Kim, D.S. Noh, Combust. Flame, 146 (4) (2006) 612-619.
[29] C. Sung, J. Liu, C.K. Law, Combust. Flame, 102 (4) (1995) 481-492.